Nanomechanical properties of multilayered amorphous carbon structures

C. Mathioudakis and P. C. Kelires
Physics Department, University of Crete, P. O. Box 2208, 710 03 Heraclion, Crete, Greece

Y. Panagiotatos, P. Patsalas, C. Charitidis, and S. Logothetidis
Physics Department, Aristotle University of Thessaloniki, 540 06 Thessaloniki, Greece

(Received 12 December 2001; revised manuscript received 26 February 2002; published 13 May 2002)

A possible route toward reducing the intrinsic compressive stress in as-grown amorphous carbon films on Si substrates, with a high fraction of tetrahedral bonding, is by forming multilayered *a*-C structures composed of layers dense and rich in sp^3 sites alternated by layers rich in sp^2 geometries, a type of an amorphous superlattice. We present here a combined theoretical and experimental effort to investigate the stability, stress, and elastic properties of this type of *a*-C material. Our theoretical approach is based on Monte Carlo simulations within an empirical potential scheme, while the experimental part consists of spectroscopic ellipsometry, x-ray reflectivity, stress, and nanoindentation measurements in films prepared by magnetron sputtering. Our central result is that the average stress in the multilayered structures is nearly eliminated through layer-by-layer stress compensation, yet the fraction of sp^3 sites in the dense regions remains high, sustained by the overwhelmingly compressive local stresses. The sp^3-rich layers are stable both against a moderate increase of the width of the low-density layers, as well as under thermal annealing. The elastic moduli of the multilayered films are comparable with those of single-layer films. This, in conjuction with their low stress, makes them suitable for mechanical purposes.

DOI: 10.1103/PhysRevB.65.205203 PACS number(s): 61.43.Dq, 61.43.Bn, 62.20.Dc, 81.15.Cd

I. INTRODUCTION

The problem of intrinsic stress in tetrahedral amorphous carbon (*ta*-C) films has attracted considerable attention in the last decade. *ta*-C is a hydrogen-free form of amorphous carbon with a high percentage of sp^3 (tetrahedral) bonded atoms.[1] Its attractive features are the wide band gap, high hardness, and biocompatibility that make it suitable for mechanical purposes. Applications include hard coatings, stiff membranes for flexural plate sensors, and as an ultrahard, low-stiction material for microelectromechanical (MEMS) developments. It is a universal finding that as-grown *ta*-C films possess high average intrinsic compressive stress. This is built up during deposition and gives rise to the adhesion failure observed at the film/substrate interface when thick layers of *ta*-C are grown. It is, therefore, desirable to reduce this stress.

The prospect of stress reduction in *ta*-C, either *in situ* or post growth, is first of all related to whether or not the high sp^3 fraction can be sustained under conditions of low stress. This matter has been the subject of a considerable debate. One point of view is that the compressive stress is the causative factor for the formation of sp^3 sites,[2,3] which implies that without a minimum critical stress the high sp^3 fraction cannot be sustained. An alternative point of view is that the compressive stress and the high sp^3 fraction in as-grown films arises from the densification during the deposition process.[4] However, this model does not tell us what would happen when the stress is relaxed.

Previous theoretical work by one of the authors[5,6] addressed this point. It has been shown that the equilibrium ground state of any *ta*-C film that relaxes the external constraints and the applied pressure (conditions imposed during deposition) corresponds to zero average intrinsic stress, yet the high percentage of sp^3 sites is maintained. This is a general result, independent of the density ρ and the mean coordination number z of the film. A prerequisite for the gradual transition to the ground state demands the film to be thick enough, so that its bulk portion is substantially larger than the interfacial region, giving it the flexibility to relax the applied pressure.

This theoretical approach offers us the opportunity to differentiate between the stressed, nonequilibrium structures formed during growth, and post-growth films that can reach their ground zero-stress state through relaxation. One possible route toward the relaxed state is through thermal annealing that provides the necessary energy to overcome the barrier between the two states, as recent experiments have shown.[7–10] The process is accompanied with small variations in bond lengths and angles without the need for conversion of sp^3 sites to sp^2 sites. Thus, the intrinsic stress is in principle not a crucial factor for the stabilization of sp^3 sites in post-growth annealed films. For as-grown films, it is still unclear whether a critical value of compressive stress is required to sustain the high sp^3 fraction as one of the models[2,3] suggests.

Another important theoretical result concerns the intrinsic stress at the atomic level.[5,6] It was found that there is an inhomogeneous distribution of atomic level stresses in *ta*-C, characterized by a high probability to find an sp^3 site under compressive stress and, analogously, by a high probability to find an sp^2 site under tensile stress. Furthermore, it was shown[6] that it is possible to preserve the local compressive stresses under relaxation-thermal annealing so as to avoid the $sp^3 \rightarrow sp^2$ transformation, while at the same time the local stresses are redistributed in such a way as to relieve the total stress in the film.

An alternative pathway of stress relaxation that has been

recently explored[11,12] is through the formation of multilayered (ML) a-C structures on Si substrates, that are composed of layers dense and rich in sp^3 geometries alternated by layers rich in sp^2 sites, a kind of amorphous superlattice. The aim is to achieve stress relaxation during growth without the need for post-growth treatment. The sp^2-rich layers in this sequential design act as a soft elastic medium under tensile or neutral stress compensating the compressive stress in the composite structure that is being accumulated due to the highly strained sp^3-rich layers. This is especially important for the interface region where excessive stress produces adhesion failure. For this reason, one starts by forming a thin sp^2-rich layer at the interface that is followed by a thicker sp^3-rich layer. This sequence is repeated several times. Care has to be taken, however, so that the introduction of the soft, graphitelike regions does not degradate the desired diamonlike properties of the composite ML structure.

The clue to the success of this design can be found in the theoretical analysis presented above. The average stress in the ML structure might be eliminated through layer-by-layer stress compensation, but the local compressive stresses in the sp^3-rich layers have to be preserved so that the sp^3 geometries remain stable. This is the crucial point. If the sp^2 layers propagate tensile stresses through lattice relaxation in the sp^3 layers and the favorable compressive conditions are overturned, then the ML structure will be transformed into a single-layer sp^2-rich film. Thus, important parameters in the ML design are the relative thickness of the sp^2/sp^3 layers and the elastic response of the interface between them.

Guided by these fundamental considerations, we carried out Monte Carlo (MC) simulations in order to investigate the stability, stress, and elastic properties of multilayered a-C structures. These simulations are complemented by and compared to spectroscopic ellipsometry, stress, and nanoindentation measurements in ML films prepared by the magnetron sputtering technique. Our aim is to associate the microscopic aspects that can be revealed by the MC simulations with the macroscopic quantities measured by experiment, to understand the important factors controlling the development of ML's, and to calibrate both the theoretical and experimental approaches for a better description of complex a-C structures.

The paper is organized as follows. In Sec. II we outline our theoretical and experimental methods of investigation. In Sec. III we give the results obtained about the structural properties, the stresses, and the elastic properties of ML structures and discuss their implications. We give our conclusions in Sec. IV.

II. METHODOLOGY

A. Theoretical methods

The theoretical investigation of the equilibrium structure and properties of a-C ML's is based on continuous-space Monte Carlo (MC) simulations. The basic underlying statistical ensemble is the isobaric-isothermal (N,P,T) ensemble, in which equilibration of a given structure is performed under conditions of constant number of atoms N in the system, constant pressure P, and constant temperature T. These conditions are the most appropriate as they mimic usual experimental conditions in the laboratory. The implementation of this ensemble for MC simulations is done through the Metropolis algorithm.[13] We have two types of moves: random atomic displacements $(s^N \rightarrow s'^N)$, where s^N is symbolic for the $3N$ scaled atomic coordinates in the cell, and volume changes $V \rightarrow V'$. These moves are accepted with the probability

$$P_{\mathrm{acc}} = \mathrm{Min}[1, \exp(-\beta \Delta W)] \sim e^{-\Delta W/k_B T}, \tag{1}$$

where

$$\Delta W = \Delta U_{\mathrm{displ}}(s^N \rightarrow s'^N) + P(V' - V) - N k_B T \ln(V'/V). \tag{2}$$

$\Delta U_{\mathrm{displ}}$ is the change in potential energy due to the atomic displacements both during the random moves and the volume changes. The volume involving terms (the last two terms) operate only during the volume changes.

It is advantageous to use the (N,P,T) ensemble because it allows volume and density fluctuations and leads to equilibration of the cell density. Thus, it avoids the *a priori* fixing of density [use of the microcanonical (N,V,E) or canonical (N,V,T) ensembles], which involves the risk of not relaxing completely the external forces and stresses applied to the system. This is particularly important at the stage of computing the system properties. However, for certain stages in the simulations, it is more convenient to use the (N,V,T) ensemble, as described below.

For the simulations we use two types of computational cells. The first type (I) is periodic in all three dimensions, with lattice parameters allowed to relax to their natural values. This type models the bulk portion of the ML's, which is overwhelmingly the largest part, deep inside the structure and away from the interface and surface regions. We have cells of two sizes belonging to this category, composed of 1760 and 2240 atoms, depending on the thicknesses of the individual layers. In the second type (II), the a-C ML is formed on top of a c-Si substrate and it is periodically repeated in the two lateral directions with lattice parameters constrained to be those of Si. The type II structure gives us the opportunity to model three different regions at the same time: close to the interface (labeled IF), the bulk layers, and near the surface (labeled S). Type II supercells contain 3680 atoms, of which 480 are Si atoms in the substrate and 3200 are C atoms in the ML.

To generate both types of cells, we start with crystalline (100) diamond monolayers in the ML [plus crystalline (100) silicon substrate layers for type II cells]. The layers to be in the sp^2-rich regions of the ML are packed at graphitelike densities, while those in the sp^3-rich regions are packed at diamondlike (and even higher) densities. The layers in the ML are liquified at $\sim$9000 K and subsequently cooled to 300 K at rates up to $\sim$40 (MC steps)/atom-K, while atoms in the c-Si substrate are kept frozen. In this part of the simulation, the (N,V,T) ensemble is invoked keeping the ML volume constant. In particular, we introduce reflective imaginary walls that separate the distinctly different region layers

and do not permit atomic diffusion between the boundaries, keeping the layer density constant during melting and amorphization. After quenching to 300 K, the walls are removed and the whole structure, including several layers of the substrate in type II cells, is fully relaxed at zero pressure with the (N,P,T) ensemble. We denote the sp^2-rich layers with A and the sp^3-rich layers with B. We have two A layers and two B layers in an $ABAB$ sequence.

The large size of the supercells does not permit the use of any other energy functional for the modelling of the interatomic interactions other than of an empirical potential. For the present investigations, the interactions are modelled via the empirical potentials of Tersoff for multicomponent systems,[14] which have been extensively tested and applied with success in similar contexts, both in strained semiconductor alloys[15,16] as well as in simulations of a-C systems.[5,6] (The multicomponent case refers to type II cells where we have, besides the elemental C-C and Si-Si interactions, the cross Si-C interactions at the interface.) The C-C interactions provide a fairly good description of a-C phases, especially regarding the energetics and derived quantities. A less good description is provided for π bonding interactions due to the lack of medium-range forces, resulting in excessively compact and dense networks at intermediate coordinations, as we shall discuss below.

The main quantities of interest in this work are the atomic level stresses and the elastic moduli of the ML's. The atomic stresses in a-C networks result due to the intrinsic disorder (local distortions of bond lengths and angles), and due to the local incompatibility that sp^2 sites feel in an environment rich in sp^3 sites, and vice versa. An extensive description of the concept of local stress and its application to a-C networks is given in a recent article.[6] The calculation of this quantity is readily done within the empirical formalism employed here, which allows the decomposition of the total energy of the system into atomic contributions. The stresses are then directly computed from the local (atomic) energetics by considering an atomic compression (tension) of the system $\sigma_i = -dE_i/d\ln V \sim p_i\Omega_i$, where E_i is the energy of atom i and V is the volume. Dividing by the atomic volume Ω_i converts into units of pressure p_i. The total intrinsic stress of the system can be calculated by summing up the σ_i over all atoms. For a completely strain compensated system the total stress is zero. This means that the individual contributions cancel each other, but it does not mean that they are themselves also diminished.

The elastic moduli are calculated with the method of homogeneous deformation. One redefines the supercell with an external strain ϵ, and the elastic modulus c is obtained from the elastic energy $\frac{1}{2}c\epsilon^2$ after all internal degrees of freedom have been fully relaxed. Specifically, for the calculation of the shear modulus $\mu=(c_{11}-c_{12})/2$, we use a volume conserving orthorhombic strain (for details see Ref. 17). The equilibrium bulk modulus at zero pressure $B_0 = V(d^2E/dV^2)_{V=V_0}$, is obtained by considering a uniform hydrostatic expansion (compression) of the system and differentiating the energy-versus-volume curve. The modulus of extension (Young's modulus) Y is calculated using the expression $B_0 = Y/3(1-2\nu)$, where $\nu = c_{12}/(c_{11}+c_{12})$ is Poisson's ratio. Formally, the elastic constants c_{11} and c_{12} are not defined for the infinite amorphous system, but one can in a schematic way calculate them for a periodic supercell with an amorphous network.

TABLE I. Properties of the single-layer a-C films deposited by MS on biased and floating substrates.

Film properties	Floating	Biased
sp^3 content (%) (from XRR)	~12	~56
intrinsic stress (GPa)	0.7	6.5
hardness (GPa)	7	24
elastic modulus (GPa)	120	200
density ($g\,cm^{-3}$)	1.9	2.62

B. Experimental methods

The multilayer a-C films were deposited at room temperature by the rf magnetron sputtering (MS) technique on c-Si (100) substrates, using a graphite target (99.999% purity) and a sputtering power of 100 W.[18,19] Additional thin single-layer a-C films were produced by the same technique as well as by electron beam evaporation (EBE). We also analyzed films that were produced at Cambridge University using the filtered cathodic vacuum arc (FCVA) technique.[20] The three deposition techniques (EBE-MS-FCVA) cover a full range of a-C films from graphitic to fully sp^3 bonded.[21] The EBE- and FCVA-produced films were used as references of highly graphitic and highly tetrahedral a-C, respectively.

No matter what the actual growth mechanisms are, the formation of sp^3-bonded carbon is generally attributed to the ion bombardment of the film surface during growth.[3,4,22–26] Especially, in sputter deposition of a-C, the ion bombardment can be achieved by applying a negative bias voltage V_b to the substrate during deposition.[18,19,26] Then, the ions provide most of their kinetic energy E to the surface and subsurface atoms of the deposited a-C film. E is the sum of the average energy of the discharge E_a and the energy provided by the electric field induced by V_b ($E = E_a + e|V_b|$, E_a being ~30 eV as measured by a Langmuir plasma probe).[27] In this process several energetic species are involved and the contribution of the carrier gas ions (Ar^+) is the most important one. It was found that a strong correlation exists between the volume fraction of Ar impurities and the sp^3 content,[26] due to the local stresses which are induced by the presence of the large Ar^+ ions.

Following this process we deposited highly graphitic a-C films (sp^3 fraction $<30\%$) on floating Si substrates (without ion bombardment) and a-C films with considerable sp^3 content (up to 50–55 %) on biased substrates ($-100\ \text{V} < V_b < -20\ \text{V}$). The properties of the a-C single layers deposited on biased ($V_b = -20$ V) and floating Si substrates are summarized in Table I.

The a-C multilayers have been grown by depositing sequential thin layers with alternating bias conditions

(floating/$V_b=-20$ V).[11,12] By starting the growth with the deposition of a thin layer on floating substrate (A-type layers), a better adhesion of the multilayer structure on the Si substrate can be achieved due to the low stress; then, a 20 nm thick layer deposited with $V_b=-20$ V (B-type layer) was grown in order to achieve a high sp^3 fraction of the whole film. The final studied films consist of three AB bilayers ($ABABAB$ structure) with total thickness ranging between 75–120 nm, depending on the thickness of the A-type layers (5, 7, 10, 15, 20 nm).

The hybridization and thickness of each layer have been studied by spectroscopic ellipsometry (SE). *In situ* spectroscopic ellipsometry spectra were obtained using a Jobin-Yvon phase-modulated ellipsometer in the spectral range 1.5–5.5 eV with a step of 20 meV. SE is a nondestructive optical technique which measures the complex dielectric function $[\tilde{\epsilon}(\omega)=\epsilon_1(\omega)+i\epsilon_2(\omega)]$ of the material.[28] However, for the case of a thin transparent film deposited on a bulk substrate, the measured dielectric function takes into account the contribution of the substrate, as well, and it is called pseudodielectric function $\langle\tilde{\epsilon}(\omega)\rangle$. The measured $\langle\tilde{\epsilon}(\omega)\rangle$ were analyzed with the Bruggeman effective medium theory (BEMT) in combination with the three-phase (air/film/substrate) model[29] using the appropriate reference dielectric functions, which describe the optical response of the fully sp^2 (Ref. 30) and fully sp^3 bonded[31] a-C. The quantitative results of the SE analysis have been validated and confirmed, for the case of the a-C single layers, by x-ray reflectivity (XRR) and x-ray photoelectron spectroscopy (XPS) studies.[26]

The density and morphology of the a-C single and multilayer structures have been studied by XRR. XRR calculates the film density (ρ) from the critical angle for total reflection θ_c through the relation

$$\theta_c^2=2N_0(e^2/2\pi mc^2)(Z\rho/A)\lambda^2, \tag{3}$$

where N_0 is Avogadro's number, A the mean atomic mass, λ the x-ray wavelength and Z the mean number of electrons per atom, e and m the electron charge and mass, respectively, and c the speed of light in air. The measured density can be also used to calculate the sp^3 content in the film, as it is proportional to the sp^3 volume fraction.[32]

The measured intensity in an XRR scan, obtained from a thin film at angles larger than θ_c, exhibits interference fringes that originate from the multiple reflections of the x-ray beam at the film/substrate interface.[32–34] These interference fringes are very sensitive to the film thickness and to the surface and interface roughness of the film due to the scattering of the x-ray beam to nonspecular directions.[35,36] Especially for the a-C multilayers, the height of the interference fringes is very much affected by the density contrast and the quality of the interfaces between the A and B layers.[12]

The XRR experiments were performed in Bragg-Brentano geometry using a Siemens D-5000 diffractometer equipped with a Goebel mirror[37] and a special reflectivity sample stage and were described in detail elsewhere.[38] The XRR measurements were analyzed using the REFSIM software and a Monte Carlo algorithm,[38] assuming a structure consisting of three identical bilayers deposited on Si (Si/$ABABAB$), with varying parameters the thickness and the density of each individual layer (A or B) and the roughness r_i of the AB interface.

The internal stress of each deposited layer has been measured by the cantilever laser beam (CLB) technique, which measures the variations of the curvature of the film/substrate system occurring due to the stress in the film. The stress σ is calculated from the difference in the curvature by Stoney's modified formula[39]

$$\sigma=\frac{E_s h^2}{6d(1-\nu_s)}\left(\frac{1}{R_s}-\frac{1}{R_f}\right), \tag{4}$$

where E_s and ν_s are the elastic modulus and the Poisson's ratio of the substrate, h and d the substrate and film thickness, respectively, and R_s and R_f the measured radius of curvature of the substrate and the film, respectively. The CLB measurements, were performed after the deposition of each layer,[11,12] using a commercial instrument from Tencor, Inc., which employs a double laser beam with 628 and 715 nm wavelength. The experimentally determined internal stress is equivalent to our calculated total intrinsic stress.

The elastic properties (elastic modulus E and hardness H) of the films were conducted using a Nano Indenter XP system with the continuous stiffness measurements (CSM) option.[40] Prior to each indentation test, two indents in 100 nm depth were conducted in fused silica to evaluate the tip condition. A detailed description of the system and the CSM depth-sensing tests have been presented elsewhere.[41] In all CSM depth-sensing tests a total of ten indents were averaged to determine the mean H and E values for statistical purposes, with a spacing of 50 (μm).

III. RESULTS AND DISCUSSION

A. Structure

We first address the structural properties of ML a-C films. We first present the theoretical results obtained by the MC simulations, and then compare them with the experimental findings.

As pointed out in the methodology section, we generated two types of ML cells, type I simulating the bulk of the material, and type II introducing interface and surface effects. The construction of both types of cells is a challenging process due to the complexity of the structures. To demonstrate that our effort was successful, we portray in Fig. 1 a three-dimensional (3D) plot of a typical bulk ML cell showing clearly the alternation of the sp^2-rich regions (layers A) with the sp^3-rich regions (layers B). In this particular cell, having an average coordination number $\bar{z}$ equal to 3.56, the layers A have a thickness of ~ 8 Å and the layers B have a thickness of ~ 24 Å. The distribution of atoms is rather inhomogeneous, characterized with a significant clustering of sp^2 sites in layers B. This is an important property of ta-C. The interfaces between the regions are not sharp. There is, instead, a continuous variation of coordination from the inner

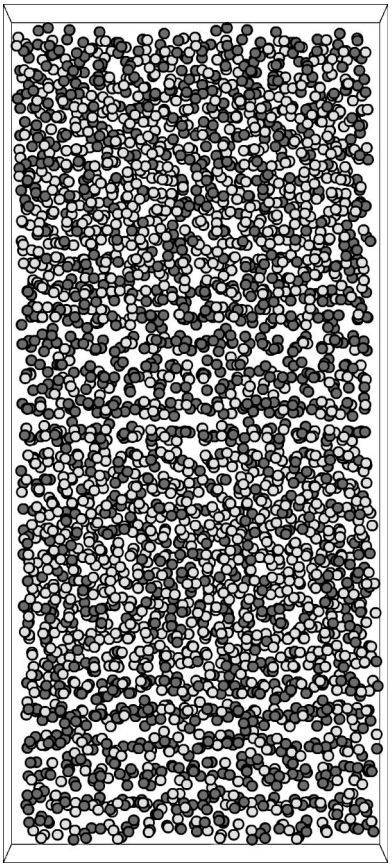

FIG. 1. Illustration of a bulk (type I) multilayered cell, periodically repeated in all directions, with a mean coordination number $\overline{z}=3.56$. Atoms are shown according to coordination: dark grey spheres denote threefold atoms while light grey spheres show fourfold atoms.

parts of the layers, where either sp^2 or sp^3 coordination prevails depending on the type of the layer, to the interface regions where there is a crossover in the dominant coordination. (Actually, during the formation of the cell, the use of the imaginary walls keeps the layer thickness and the interfaces sharp, but this changes when the walls are removed and the structure is relaxed.)

A more quantitative picture of this transition is obtained by partitioning the ML cell into thin slices (of thickness equal to 3 Å) in the vertical direction and computing the fractions of sp^2 and sp^3 sites in each one of them. The results of this analysis, for the cell described above, are given in Fig. 2 which plots the relevant fractions with respect to the depth z in the ML. The maximum fraction of the sp^3 sites (70–75 %) occurs deep in the middle of layers B and its minimum (20%) in the middle of layers A, and vice versa for the sp^2 fraction. The average fraction of sp^3 sites in regions B is $\sim$60% and in layers A $\sim$30%. We could somewhat loosely specify the interface boundaries at the positions where the sp^3 and sp^2 distributions cross each other. The density of layers A is $\sim 2.5\ \mathrm{g\,cm^{-3}}$, that is graphitelike, while that of layers B is $\sim 3.3\ \mathrm{g\,cm^{-3}}$, that is diamondlike.

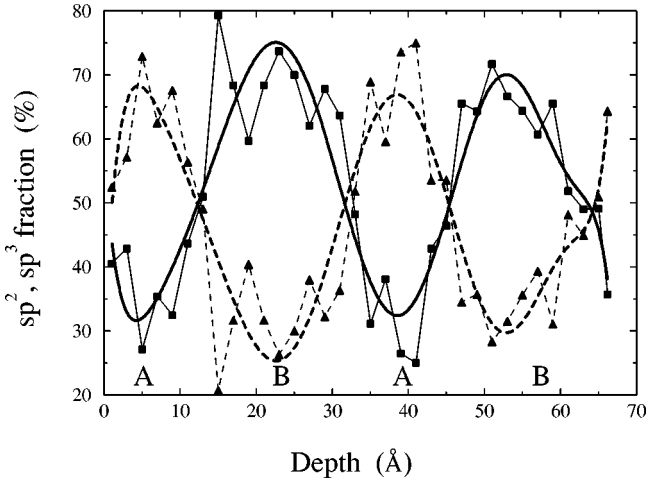

FIG. 2. Variation of sp^3 and sp^2 fractions as a function of depth z in the $ABAB$ ML cell shown in Fig. 1, averaged in thin slices of width of 3 Å. The squares and solid line denote the sp^3 variation, while the triangles and dashed line show the sp^2 variation. The thick solid and dashed lines are polynomial fits to the respective points.

The same overall trends and a clear distinction between A and B layers are found in all ML's studied. The sp^3 fraction in layers B depends rather weakly on the relative thickness ratio $d(A/B)$. For example, it is reduced to $\sim$53% when $d(A/B)$ is nearly 1/2, compared to 60% in the 1/3 case discussed above. This shows the stability of layers B against increasing the width of layers A (which of course remains smaller than the width of layers B). We also checked the thermal stability of the ML structures by annealing them at higher temperatures and then cooling them back to 300 K. This check is important especially for layers B, where it is essential to preserve the high sp^3 fractions. We found that the ML's are stable up to $\sim$1000 K. Beyond this point there is a massive transformation of sp^3 sites into sp^2 sites, consistent with earlier findings,[42] signifying a graphitization of the whole structure.

At this point, we would like to discuss in some detail some reports in the literature[43–46] arguing that simulations with the Tersoff potential at typical ta-C densities ($\geqslant 3\ \mathrm{g\,cm^{-3}}$) underestimate the sp^3 fraction by almost a factor of 2. For example, Stephan and Haase (SH) (Ref. 44) found in molecular dynamics (MD) simulations that at a density of $3\ \mathrm{g\,cm^{-3}}$ the sp^3 fraction is 34%. Marks[43] interpreted this result as indicating severe underestimation of tetrahedral bonding with the Tersoff potential. However, MC simulations with this potential have repeatedly found sp^3 fractions well exceeding 70%.[5,6] At this specific density ($3\ \mathrm{g\,cm^{-3}}$), networks were generated with $\sim$50% sp^3 bonding. At $3.2\ \mathrm{g\,cm^{-3}}$ the MC networks contain about 78% sp^3 sites. Thus, it seems that the MC simulations and those of SH contradict each other. This requires an explanation.

The answer to the paradox lies in the kind of statistical ensembles used in the two simulations. In the MD simulations of SH, as in most MD simulations, the microcanonical (N,V,E) ensemble is used. This means formation of the

amorphous structure during quenching at zero applied pressure. This fact has been pointed out by SH. To the contrary, the MC simulations, carried under the (N,P,T) ensemble, form the amorphous network under applied pressure, which stabilizes the sp^3 bonding, without fixing *a priori* the density. At the final stage, when cooling is completed and equilibration is taking place, the pressure is removed and the density comes out as a result of the simulation. Actually, the MD and MC simulations are not directly comparable because relaxation of the constant-volume constraint in the MD simulations would lower the density of the network. According to our estimates,[5] a 34% sp^3 fraction corresponds to a relaxed density of ~ 2.9 g cm^{-3} with the Tersoff potential. Still, this density estimate is an overestimation. It is a result of the absence in this potential of an explicit π bonding term that would treat properly π repulsion and give to the network the correct density. This problem is more serious for low- to intermediate-sp^3 content networks, where π bonding is predominant, and less in ta-C networks. In the latter, the density is overestimated by ~ 3–4 %.

So, it is possible to construct high-sp^3 content networks with the Tersoff potential by quenching *under pressure*. Values as high as 2–3 Mbar have been used in the past in order to achieve this.[5,6] (The equivalent in the NVE or NVT case is to generate a liquid at superdiamond densities; after quenching and amophization, however, the volume and density has to be relaxed.) The pressure is needed to overcome the barrier between sp^2 and sp^3 sites.[42] It does also help to avoid numerous artificial configurations mixing threefold- and fourfold-coordinated atoms, that arise due to the absence of π bonding terms. The resulting structures, after pressure release and density equilibration, are metastable with respect to transformation of sp^3 to sp^2 sites, but only at high temperatures (1100 K) as we have shown in the past,[5,42] and in agreement with experiment. To the contrary, none of the other liquid-quenching MD simulations reporting high-sp^3 contents, using either *ab initio* forces[47,48] or other empirical potentials,[43] have been able to probe the stability of ta-C networks as a function of temperature.

ta-C films are usually grown on Si(100) substrates. In order to include the substrate/film interface (IF) effect on the ML, and to have a more direct comparison with our experimental observations, we also analyzed cells of type II. A typical ''epitaxial'' c-si/$ABAB$ cell is portrayed in Fig. 3. The total thickness of the film is ~ 75 Å. We clearly see that the depicted structure exhibits the desired modulations in coordination. A comparison to the bulk cell of Fig. 1, shows that there are some structural differences at the IF region and at the surface region, as expected. Most notable are the enrichement of the interface region with sp^3 atoms, in the otherwise sp^2-rich layer A, and the enrichement of the surface in the top B layer with sp^2 atoms, a feature of ta-C that is by now well established both by experiment[49] and by theory.[50,51] The two inner, bulk layers B and A have more or less similar structural characteristics in both types of cells.

An alternative way of looking into how the sp^2 and sp^3 atoms are distributed in the film is the following. We compute the unnormalized probabilities of finding threefold and fourfold atoms at depth z, which measures the distance from the interface to the surface of the multilayered structure. These probabilities are defined as the atomic-position densities of states $P(z)=dN/dz$, where dN is the number of sp^2 or sp^3 sites lying in the vertical position interval between z and $z+dz$. The resulting distributions are shown in Fig. 4. The thick lines are polynomial fits to the very fine mesh of $P(z)$. Indeed, the probability for finding sp^3 atoms is markedly pronounced in the two B layers, while that of sp^2 atoms is larger in layers A. Still, there is an appreciable amount of sp^2 atoms in the B layers (it is quantified below). A third peak in panel (a) shows that the surface is enhanced with sp^2 atoms, in accordance with the visual inspection of Fig. 3. An interesting effect is that the center of gravity of the sp^2 distribution in the first of the A layers is shifted towards the interface which is rich in sp^2 atoms. This is in agreement with experimental work.[49] The other interesting feature appears in panel (b), namely, a tendency for sp^3 atoms to gather near the interface, as we discussed above, when the rest of the A layer is almost depleted from them. A close inspection of the interface region shows that this effect is driven by the tendency of carbon atoms to preserve the tetrahedral arrangements of silicon atoms in the topmost layer of the substrate. Thus most of these tetrahedral carbon atoms participate in SiC-like geometries.

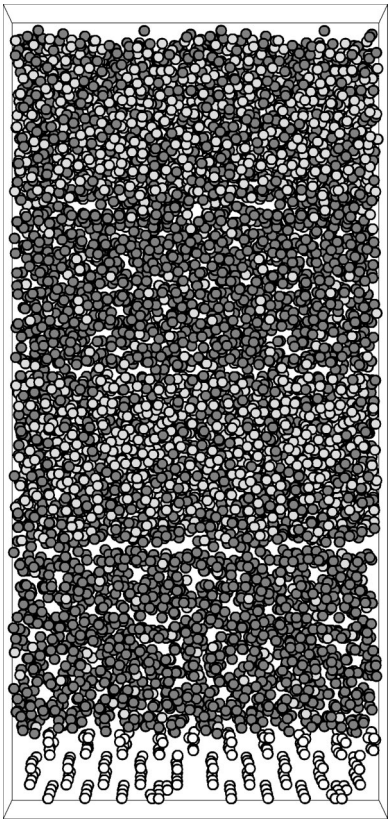

FIG. 3. Illustration of an epitaxial (type II) ML cell, periodically repeated in the two lateral directions. Open spheres show Si atoms in the substrate. Light grey (dark grey) spheres show fourfold (threefold) carbon atoms in the ML, respectively.

Following the partitioning procedure described above for the bulk cell, we compute the sp^3 fraction and density in thin

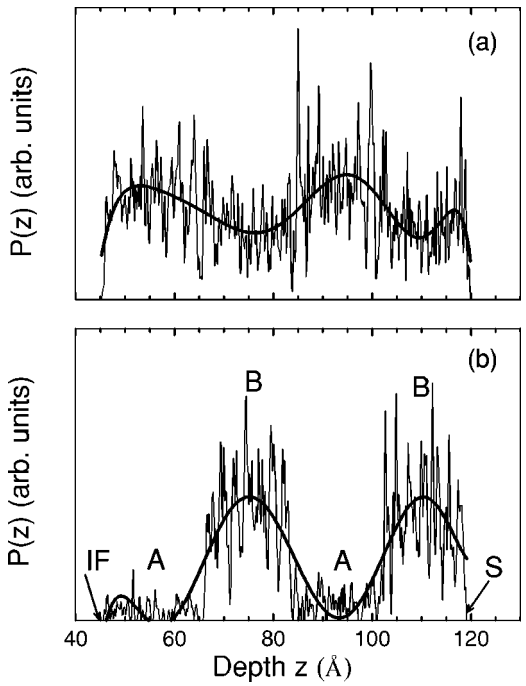

FIG. 4. Position probabilities vs depth (see text), at 300 K, in the *ABAB* ML structure shown in Fig. 3. The interface (IF) with the Si substrate and the free surface (S) are denoted by arrows. (a) For sp^2 atoms. (b) For sp^3 atoms.

slices (3 Å) across the *c*-Si/*ABAB* ML. The results are given in Fig. 5. The maximum sp^3 fraction in the *B* layers reaches ~70%, while in the *A* layers is ~10%. This is somewhat lower than in the bulk case, and reflects the effect of the surface and interface environments. Tensile stress conditions in these areas disfavor the formation of sp^3 sites. The

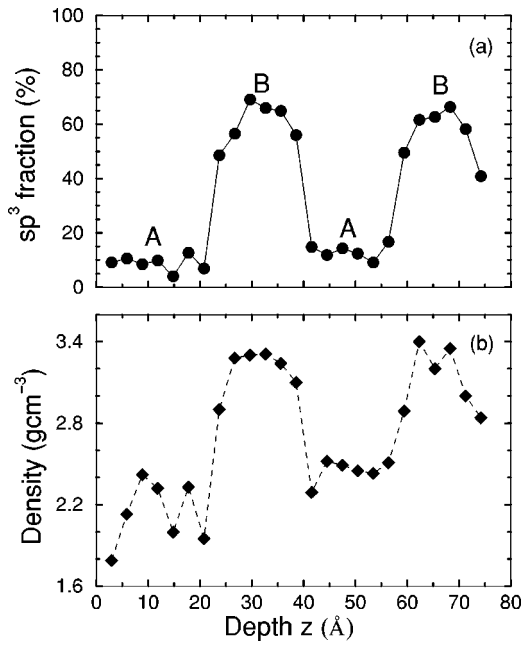

FIG. 5. Variation of the sp^3 fraction (a) and of the mass density (b) in the multilayered structure shown in Fig. 3.

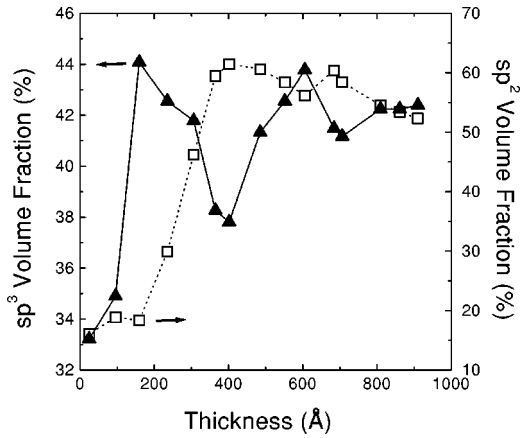

FIG. 6. Variation of the sp^3 and sp^2 fractions in a representative multilayered *a*-C film as a function of the film thickness *z* (the Si substrate is at $z=0$). The individual sp^3- and sp^2-rich layers are easily identified, though the current SE analysis underestimates much the sp^3 fraction.

density variations follow closely the respective variations of the sp^3 fraction in the multilayers. The *B* layers are quite dense with certain slices reaching a density of ~3.4 $\mathrm{g\,cm^{-3}}$. (Diamond has a mass density of 3.51 $\mathrm{g\,cm^{-3}}$.) As we explained above, these values are overestimated for the sp^3 fractions at hand. More appropriate estimates would be about 3.2 $\mathrm{g\,cm^{-3}}$.

The experimentally produced multilayer cells are bigger than the calculated ones. The thickness of the whole multilayer structure ranges from 750 to 1200 Å, and those of the individual layer is between 50–200 Å. The high thickness of the produced cell has been chosen in order to get the highest possible accuracy and to avoid the inherent limitations of the characterization techniques (SE and XRR). Although there is a different scale for the dimension of the experimental and calculated cells, there is good qualitative agreement between the experimental and calculated results.

From the SE data analysis using the Bruggeman effective medium theory[29–32] we obtained the film composition (sp^2, sp^3 fractions) and the thickness *d* of each deposited layer. We have found that the sp^2 and sp^3 fractions exhibit a modulation versus the film thickness. The modulation period depends on the bias voltage applied to the substrate. Figure 6 shows the depth profile of the sp^3/sp^2 content *versus* the thickness *z* ($z=0$ refers to the Si substrate), based on the results of BEMT analysis, for a representative *a*-C multilayer structure deposited by MS. The individual sp^3- and sp^2-rich layers can be easily identified, though their interfaces are not quite sharp. The sp^3/sp^2 ratio increases in the *a*-C multilayers when $V_b<0$ V and decreases when $V_b>0$ V (floating substrate). The values of the sp^3 content in the individual layers were found to be somewhat lower than the ones in the single layer films deposited with the same conditions.[26] This underestimation of the sp^3 content is due to the rough *AB* interfaces that cause light scattering, which misleads the BEMT model to translate it as optical absorption in the vis-UV spectral region, overestimating the content of

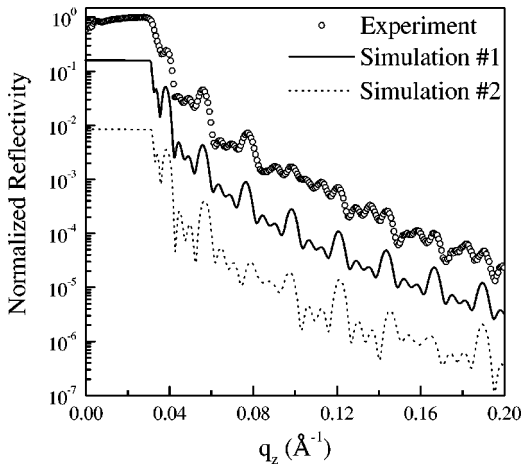

FIG. 7. XRR diffractogram from a representative *a*-C ML structure deposited by MS and two simulations assuming either rough (No. 1) or smooth (No. 2) interfaces between the individual layers. The simulated curves are shifted to lower values.

sp^2-bonded *a*-C. Nevertheless, SE can provide the qualitative profile and a good quantitative approximation of the sp^3/sp^2 variation within the individual *A* and *B* layers, as shown in Fig. 6.

In addition to SE, the *a*-C multilayers were examined in more detail, concerning the individual thickness of the layers *A* and *B*, by XRR and transmission electron microscopy studies in cross section geometry (XTEM).[12] The cross examination of the *a*-C multilayers by the above three techniques provides the following: (i) a very good agreement between the three techniques concerning the total film thickness and the modulation period λ (i.e., the thickness of the *AB* bilayer) and (ii) a difference in the thickness of the individual *A* and *B* layers was detected between XRR/XTEM and SE. The thickness of the *A* layers found by XRR/XTEM were smaller than the ones deduced by SE.

In order to identify the origin of this difference between SE and XTEM/XRR a BEMT model using a stratified *a*-C structure was employed.[11,12] Thus, we examined the effect of layer *B* (*A*) when deposited on layer *A* (*B*), assuming that the film consists of separated layers and taking into account only the last two layers of the growing film (the previous layers were frozen). Following this analysis, we can discern a thickness reduction in layers *A* (rich in sp^2 bonds), of 30–40 Å, caused during the deposition of the layers *B*. This thickness reduction in layers *A*, when a layer *B* is deposited, can be attributed to either the partial transformation of top sp^2 bonded material to sp^3 one, due to the stress field originating from the *B* layer and applied to the top of the sp^2-rich layer, or to the densification of layer *A* due to the intense Ar^+ ion bombardment.[19,26]

On the other hand the deposition of layers *A* on the top of layers *B* was found to cause no measurable thickness reduction of layers *B*. The XRR analysis confirms this partial transformation of the top sp^2-rich layer to sp^3 rich in terms of the roughness of the *A*/*B* interface. Figure 7 shows the x-ray reflectivity vs the x-ray scattering factor $q_z = 4\pi(\sin\theta)/\lambda$, where θ is the angle of incidence and λ the x-ray wavelength measured in nm. Three curves are shown: an experimental (open circles) from a representative *a*-C multilayer and two corresponding Monte Carlo simulations assuming either rough (solid line) or sharp (dotted line) *AB* interfaces. The simulated curves are shifted to lower values for demonstration purposes (to show better the line shape). The interference fringes manifesting in the experimental XRR curve are not so sharp as they would be expected for a sharp *AB* interface. Instead, the Monte Carlo simulation of the XRR curve assuming a rough interface follows better the experimental data (open circles) and is in qualitative agreement with the computational results (Figs. 2,4). According to the Monte Carlo simulations of the XRR curves, the *AB* interface roughness is $r_i = 40$ Å.

TABLE II. Properties of the individual layers of the ML cells deposited by MS, according to XRR analysis. Listed are the density, the sp^3 fraction, and the *AB* interface roughness.

Layer	ρ(g/cm^3)	sp^3(%)	r_i(Å)
sp^2 rich	2.0	18.0	40.0
sp^3 rich	2.5	48.5	

The results of the properties of the individual sp^2-rich and sp^3-rich layer in the ML structure, based on XRR results, are summarized in Table II. An interesting feature of these results compared with the properties of the *a*-C single-layers deposited with the same conditions (Table I) is that the density values are slightly different. Thus, the sp^3- (sp^2)-rich layers in the ML structure are slightly less (more) dense than the corresponding single layers, respectively. This may be another indication of local transformations in the whole ML structure in order to relieve the mean intrinsic stress of the overall structure, as we shall discuss below. Let us also point out that the density and the fraction of sp^3 sites in films prepared by magnetron sputtering is, in general, lower than the corresponding values obtained by techniques such as cathodic arc or pulsed-laser deposition. Nevertheless, the crucial point is that the density and the sp^3 fraction of ML films are sustained, with respect to the same quantities in single-layer films, prepared by magnetron sputtering, while stress is lowered. This is shown at an even more quantitative manner by the MC simulations. So, we would like to stress that the realization of multilayered films with the desired properties is a general procedure, which is not limited to the present experimental method, but can be used in conjuction with the other experimental techniques as well.

B. Intrinsic stress

The stress field in the multilayered structures is considerably more complicated than in single-layer *ta*-C films. Let us first look at our computational results. A site by site analysis of the stress field, as it is varied through the *ABAB* layers, is provided by calculating the atomic level stresses in the way outlined in the methodology. A 3D plot showing the atomic stresses (shaded according to magnitude and sign) in a type-I ML cell ($\bar{z} = 3.56$) is given in Fig. 8. It is clear that compres-

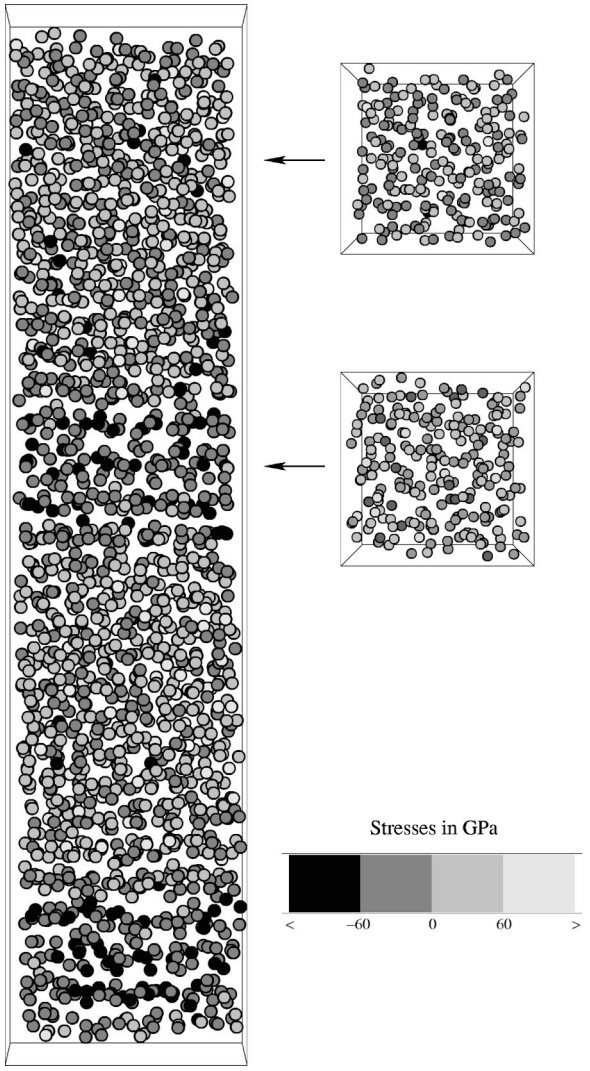

FIG. 8. Atomic positions in the ML cell, also shown in Fig. 1, shaded according to the local atomic stress (left). Also shown are stresses in typical single-layer cells with the same z as in layers A and B of the ML (right). Positive sign denotes compressive stress.

sive stresses dominate in layers B, while tension is overwhelmingly the dominant stress condition in layers A. A close inspection of the interface regions reveals that a gradual transition from tensile to compressive stress, and vice versa, is taking place. These properties were rather expected, since we have found in the past that local compressive (tensile) stresses favor the formation of sp^3 (sp^2) sites, respectively.[5]

An interesting feature is revealed by comparing the stress conditions in the A and B layers of the ML with the stresses in typical bulk single-layer cells, fully relaxed with respect to external constraints, which have approximately the same coordination number $\bar{z}$ with the respective ML layers, as shown in Fig. 8. It comes out that there are excessive stress conditions in the ML layers, compared to the single-layer cells. In the latter case, the spatial distributions and magnitude sign of stresses is such that the average stress in the cells, both sp^3- and sp^2-rich, balances to about zero.[5,6] (Still, the average stress over the fourfold atoms is compressive, while that of

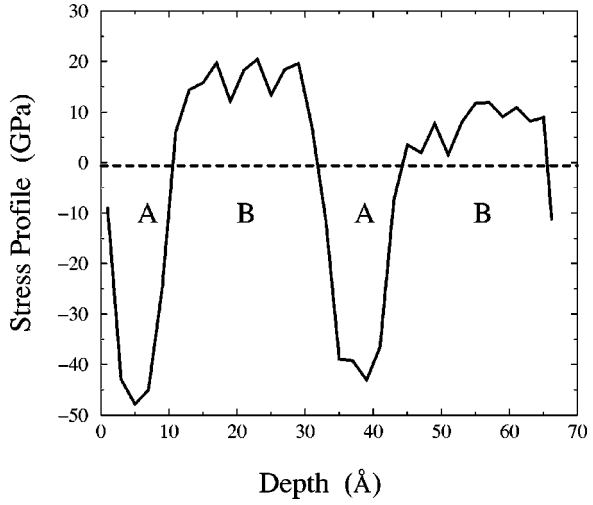

FIG. 9. Variation of atomic stresses in the ML of Fig. 8, averaged over thin slices of 3 Å width, as a function of depth. The average stress in the structure is denoted by the dashed horizontal line.

threefold atoms is tensile.) In the ML case, the vast majority of atoms in layers A are under high tensile stress, and averaging within the layer seems not to lead to a compensated state. A similar picture applies to layers B.

To quantify this observation, we compute the stress within thin slices (3 Å) in the vertical direction of the ML, by averaging over the local stresses in the slice. The stress profile for the ML discussed above is shown in Fig. 9. The stress variations confirm that layers A are under excessive tensile stress which is peaked within the slices lying in the middle. Note the smooth and gradual change of stress conditions to compressive as we move into the sp^3-rich regions. It is clear that the average stress in each individual layer A or B is not compensated but attains a definite tensile or compressive value.[52] Still, the average stress over the whole bulk ML cell is calculated to be practically zero within the accuracy of the calculation (it is less than 1 GPa). This shows that the compressive stresses in layers B are compensated by the tensile stresses in layers A. The analogous effect in single layer ta-C films requires the mostly tensile local stresses at sp^2 sites to compensate the compressive stresses at the sp^3 sites.

A similar situation is observed in the type-II ''epitaxial'' cells. To trace the strain field, in this case, let us compute the probability of finding an atom (no distinction between sp^2 and sp^3) under tensile or compressive stress at depth z, independent of its magnitude, in a similar manner used for the position probabilities of Fig. 4. So, we compute the atomic stress densities of states $P(\sigma)=dN/dz$, where dN is the number of sites under tensile or compressive stress lying in the vertical position interval between z and $z+dz$. The resulting distributions are shown in Fig. 10. The central outcome of this analysis is that tensile stress is predominant in layers A, where the sp^3 fraction is low, while compressive stress is maximized in layers B where the sp^3 fraction is high. It is instructive to compare Figs. 4 and 10. It is obvious that the position and stress distributions exhibit the same pattern, which shows that the relation between stress condi-

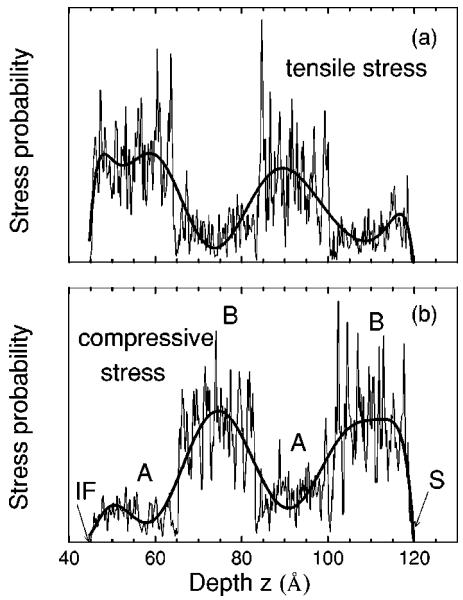

FIG. 10. Stress probability distributions (in arbitrary units) as a function of depth in the epitaxial cell shown in Fig. 3. The interface (IF) with the substrate is on the left and the surface (S) is on the right. The thick lines are polynomial fits. (a) Tensile stress probability. (b) Compressive stress probability.

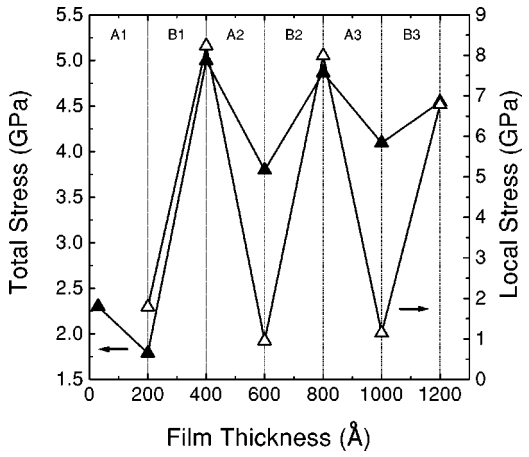

FIG. 11. The evolution of average stress (solid triangles) *versus* thickness for a film deposited with alternating V_b. Open triangles represent the stress within the individual layers. The vertical dotted lines separate the six regimes referred to the layers *A* and *B*.

tions and hybridization has a global character. Other notable features in Fig. 10 are the peaks in the tensile stresses at the interface (IF) and the surface (S), and also the small peak in the compressive stress in layer *A* near the interface. Again, this is consistent with the enhanced sp^3 population seen in Fig. 4 in the region adjacent to the interface.

The average stress over the whole *ABAB* ML cell, excluding the substrate, is also nearly relaxed, it is ~ 2 GPa. So, as a general finding, we can say that the tensile stresses, particularly in layers *A*, balance overall the high compressive stresses in layers *B*, but at the local level the compressive stresses are preserved and so is the sp^3 fraction in the *B* layers. This characteristic makes the multilayered structures promising candidates for solving the adhesion problem, without rendering the desired diamondlike properties.

We now proceed to examine the stress conditions observed in our experimental studies. The stress behavior during the experimental development of *a*-C multilayers with alternating V_b is of great importance. The main characteristic of the *a*-C multilayers deposited by MS is that they exhibit always compressive stresses, even when they are sp^2 rich. Therefore, the difference in stress behavior between the sp^2- and sp^3-rich *a*-C layers, deposited by MS, does not lie in their character (tensile or compressive) but in the values of compressive stresses (see Table I and Ref. 19). Thus, no quantitative comparison of the experiments with the computational results can be made. However, the experimental stress variation in the *a*-C multilayers share many qualitative features with the computational results, as it has been shown for the density and sp^3 content.

Figure 11 shows the evolution of the average stress (solid triangles) with the thickness z ($z=0$ refers to the *a*-C/Si interface) for a typical *a*-C multilayer deposited with alternating V_b. The average stress exhibits the same modulation with the sp^3 content as V_b alternates from floating to -20 V (see Fig. 6). The vertical dotted lines are used just to distinguish the regimes referred to the different layers *A* and *B*. The first regime describes the stresses in layer *A*, which consists of two sublayers: the first at the very initial stages of growth (~ 30 Å) to describe the stress conditions close to the interface and the second at the thickness of 200 Å to describe the stress conditions of the bulk *A* layer.

The compressive stress close to the interface is higher than in the bulk of the *A* layers, in perfect agreement with the existence of a peak in the computational results of Fig. 10(b) regarding the compressive stress in the *A* layer. Afterwards, the stress reduces due to the development of the continuous sp^2-rich layer. When the layer *B* is deposited with negative V_b, the compressive stress increases progressively to 4.8 GPa, that is well below than the stress (6.5 GPa) of the single layers deposited with the same conditions (see Table I and Ref. 19). At this stage the deposited material exhibits different composition (rich in sp^3 sites) than the layer *A* (rich in sp^2 sites), as shown in Fig. 6. The deposition of another layer of type *A* leads again to a stress reduction of ~ 0.6 GPa followed by an increase in the stress level when the next layer *B* is deposited, in fair agreement with the simulated epitaxial cell of Fig. 3 and the corresponding computational results of Figs. 5 and 10. The same stress dependence on the V_b is also obtained when we deposit the third *AB* bilayer.

For a better understanding of the stress behavior we calculated the stress within the individual layers and the results are also shown (open triangles) in Fig. 11. These results show that the *A* and *B* layers exhibit a local stress level about 1 and 7.5 GPa, respectively. On the other hand, the saturation level of the total stress, shown in Fig. 11 (solid triangles), is about 4.5 GPa, that is well below the 6 GPa obtained in *a*-C single layers with similar mean coordination number. That is, the interposition of the low-stressed *A* layers seems to promote the control of the total stress level in the *a*-C multilayers. Although the total stress is lower in *a*-C multiple layers

TABLE III. Elastic moduli (in GPa) of four computer generated multilayered cells, characterized by a different mean coordination number $\overline{z}$, at 0 K. Listed are the bulk modulus B_0, the Young's modulus Y, the shear modulus μ, and the two elastic constants c_{11} and c_{12}.

$\overline{z}$	B_0	Y	c_{11}	c_{12}	μ
3.44	267	612	632	85	273
3.51	287	658	679	91	294
3.56	302	692	715	96	309
3.64	317	727	750	100	325

than in the single layers, the former still exhibit a high fraction of sp^3-bonded a-C. This supports our computational results according to which, the key factor for the stability of the sp^3 sites is the local stress and not the total stress of the multilayer structure.

C. Elastic properties

One of the most important diamondlike properties of ta-C is high hardness. A crucial question then arises. Do the ML structures studied here retain the high values of elastic moduli, characteristic of ta-C films, or does the introduction of sp^2-rich layers lead to the deterioration of their hardness? To answer this question, we calculated the elastic moduli of a number of type-I (bulk) cells, characterized by different average coordination numbers z, and compared them with the corresponding moduli of single-layer cells and also with the experimental nanoindentation measurements. From this comparison, some interesting conclusions are reached.

The results of our calculations for a number of moduli and elastic constants are listed in Table III. We also plot in Fig. 12 the variation of B_0 as a function of z and compare it with the corresponding variation in the single-layer case. There are two notable aspects of these results. First, we observe that the ML structures have somewhat lower moduli than the single-layer films. Yet, the decrease is rather small and does not show any appreciable degradation of hardness. Note that

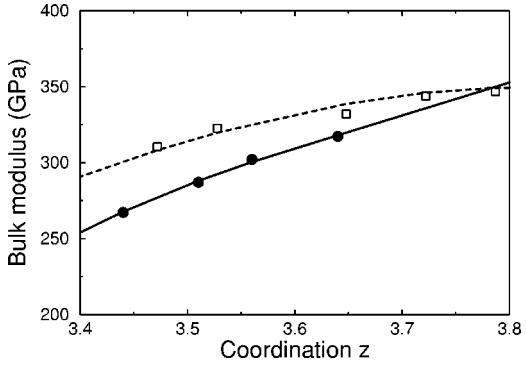

FIG. 12. Variation of the calculated bulk modulus of ML cells (filled circles) as a function of the mean coordination z, contrasted to the respective variation in single-layer cells (open squares). The dashed line is a fit to the latter, while the solid line fits the former and is extrapolated to larger z.

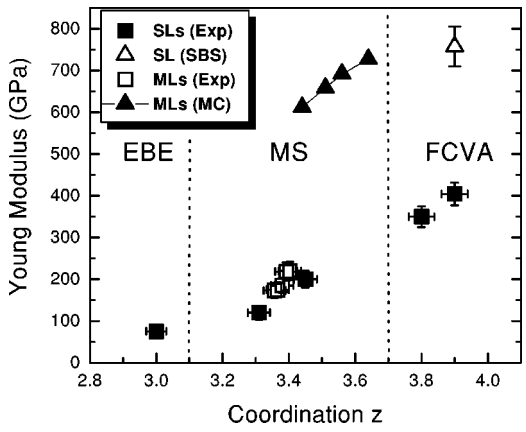

FIG. 13. The variation of Young's modulus with the mean coordination number for a-C multilayers (ML's, open squares) and for single-layers (SL's, filled squares) based on CSM data analysis. The various growth techniques are also indicated for each case. Solid triangles show the corresponding MC calculations for the multilayer cells. The SBS result of Ferrari *et al.* (Ref. 55) for FCVA is also shown (open triangle).

as z increases the difference becomes smaller and the ML variation, by extrapolation, converges to the single-layer variation. This, however, would occur at a z exceeding 3.75, a limit at which the ML transforms into a single-layer film because the sp^2-rich layers shrink and disappear. (Recall that z denotes the mean coordination of the whole ML cell.) For $z=3.64$, the highest coordination that we have been able to achieve, the moduli are quite high, showing that as-grown ML's, designed this way to have low intrinsic film stress, are suitable for mechanical purposes.

The experimentally determined elastic properties of various a-C ML's, namely, hardness and Young's modulus, have been measured by nanoindentation employing the CSM technique.[40,41] The A layers of the studied ML films have a variable thickness. For this reason, the mean coordination number of the whole ML structure was calculated from the density values and the thickness of each individual layer, measured by XRR, assuming a linear correlation between density and coordination number based on Refs. 26,32.

In addition, CSM was used to study the elastic properties of representative a-C single layers 25–30 nm thick, which were deposited by various techniques (EBE, MS, FCVA) covering a wide range of mean coordination number (calculated from the density values). As the single layers are very thin, there is considerable effect from the Si substrate in the measured elastic modulus values.[21] In order to separate the elastic properties of the film from those of the substrate and the influence of the tip's radius effect, we fitted the experimental results with two empirical equations based on finite-element analysis to get the real elastic properties of the a-C films.[21,53]

Figure 13 shows the variation of the Young's modulus Y with the mean coordination number (calculated from XRR) for the a-C multilayers and single layers based on CSM data analysis. In both cases, the modulus increases considerably with the mean coordination number, in qualitative agreement with the computational results for B_0 shown in Fig. 12, or

equivalently with the computed Young's modulus results for the MLs, shown in Fig. 13. However, despite the agreement on the overall trend, there seemingly is a considerable quantitative difference between the experimental and theoretical results.

There are a number of reasons for this quantitative difference. First, the computed elastic moduli are for type-I (bulk) cells without any contribution from the interface and surface regions, which become important for thin films, while the experimentally determined moduli unavoidably reflect contributions from these regions. (There are inherent difficulties in measuring the elastic properties of very thin films.)[21] Secondly, it has been recently reported[54] that the Tersoff potential used for the simulations overestimates the moduli of single-layer cells in the intermediate region $3.3<z<3.6$, by $\sim 18-24\,\%$ when compared to more accurate tight-binding approaches. This indicates excessively compact networks at these coordinations, as we noted above. Thus, correcting for a similar overestimation in the case of the ML cells, we estimate Y to be in the range of 490–620 GPa. On the other hand, previous calculations[5] of Y with the Tersoff potential at coordinations relevant to ta-C ($z \simeq 3.8-3.9$) yielded values near 800 GPa, in excellent agreement with the values 750–790 GPa reported by Ferrari *et al.*[55] for FCVA films, determined by surface Brillouin scattering (SBS). Also, the corresponding calculated bulk modulus $\simeq 360$ GPa (Refs. 5,6) agrees well with the SBS measurements (368 GPa) of Manghnani *et al.*[56] in ta-C films synthesized from C_{60} under pressure. Therefore, as the comparison of the SBS (Ref. 55) and the present nanoindentation measurements of Y in Fig. 13 shows, it is likely that the latter method underestimates the elastic moduli by more than 40%.[7,55,57,58] Taking this into account would raise the moduli of our experimental ML films to values quite close to the corrected theoretical ones.

Another interesting comparison of our simulational and experimental results, concerns the question of whether the moduli of the ML structures are enhanced or not with respect to the moduli of single-layer films with the same mean coordination number. The computational results of Fig. 12 show that the bulk modulus of the ML's slightly degrades with respect to the single-layer case. On the other hand, the experiment (Fig. 13) shows a small enhancement of the elastic modulus of the ML structures. This difference in the trend cannot be attributed to the systematic inaccuracies (outlined above) in the methods involved, but it rather points to some inhomogeneous patterns (nanostructured grains) in the experimental ML films[12,59] that harden the material, and which are less pronounced in the single-layer films. (Such structures are absent in the simulational cells.) For example, it has been reported[60,61] that the existence of nanostructured regions in ta-C films prepared by pulsed-laser deposition enhances their hardness. The problem of nanostructured and/or nanocrystalline seeds in a-C is not yet well understood, and further experimental and theoretical work is needed to elucidate the properties of this complex material.

IV. CONCLUSIONS

Monte Carlo simulations of the structure, local stress fields and elastic moduli, in conjuction with experimental probes, such as spectroscopic ellipsometry, XRR, stress measurement techniques, and nanoindentation, have led us to an in-depth analysis of ML a-C films that are composed of layers dense and rich in sp^3 sites alternated by layers rich in sp^2 geometries. The simulated structures were generated by appropriate liquid-quenching methods, while the experimental films were grown using the magnetron sputtering technique.

The structural analysis of the simulated (grown) ML films shows a clear alternation of the sp^2- and sp^3-rich layers, with a continuous variation of coordination from the inner parts of the layers to the interface regions. The layer densities show similar variations. A tendency of sp^3 atoms to gather near the interface with the substrate is observed, while the surface is enriched with sp^2 atoms. The percentage of sp^3 atoms in the dense layers rises up to $\sim 70\%$ in the simulated structures, and up to $\sim 50\%$ in the deposited films. In both cases, the density and sp^3 fraction in the dense layers are comparable with the values in single-layer films.

The analysis of the stress fields reveals, in accordance with the coordination variations, a gradual transition from compressive stress in the dense layers to low, or even to tensile stress (in simulated cells) in the sp^2-rich layers. The total stress is completely compensated in the simulated cells. In the sputtered films, the total stress is lower than in single-layer films with similar mean coordination number. Thus, both the computational and experimental results indicate that the key factor for the stability of the sp^3 sites is the local stress and not the total stress of the ML structures.

The calculated elastic moduli, after correction for overestimation in the intermediate coordination region, are quite high making them suitable for mechanical applications. They are only slightly degraded with respect to the moduli of single-layer films. On the other hand, the experimental moduli, measured by nanoindentation, are lower than the simulational values. This indicates an already pointed out by other authors problem, namely, that nanoindentation underestimates the moduli when compared to acoustic wave techniques, such as the surface Brillouin scattering method. Also, the experimental ML moduli are slightly enhanced with respect to the moduli of single-layer films. We interpret this in terms of the existence of nanostructured grains in the sputtered films. Finally, we emphasize that the idea for the realization of multilayered films, as a mean to relieve the stress in the ta-C material, is not limited to the present experimental method, but it can be used in conjuction with other experimental techniques, such as cathodic arc and pulsed-laser deposition, that yield higher densities and sp^3 contents.

ACKNOWLEDGMENTS

The FCVA samples were kindly provided by John Robertson's group at the Engineering Department, University of Cambridge. This work was supported in part by a ΠΕΝΕΔ 1999 Grant No. 99 ΕΔ 645, from the Greek Generel Secretariat for Research and Technology.

[1] Recent reviews of the state-of-the-art can be found in *Amorphous Carbon into the Next Millenium, Proceedings of the Second International Specialist Meeting on Amorphous Carbon* (SMAC'99) [Int. J. Mod. Phys. B **14** (2000)]; *Proceedings of the Third Specialist Meeting* (SMAC 2000) [Diam. Relat. Mater. **10** (2001)].
[2] D.R. McKenzie, Rep. Prog. Phys. **59**, 1611 (1996).
[3] D.R. McKenzie, D. Muller, and B.A. Pailthorpe, Phys. Rev. Lett. **67**, 773 (1991).
[4] J. Robertson, Diamond Relat. Mater. **2**, 984 (1993).
[5] P.C. Kelires, Phys. Rev. Lett. **73**, 2460 (1994).
[6] P.C. Kelires, Phys. Rev. B **62**, 15 686 (2000).
[7] T.A. Friedmann, J.P. Sullivan, J.A. Knapp, D.R. Tallant, D.M. Follstaedt, D.L. Medlin, and P.B. Mirkarimi, Appl. Phys. Lett. **71**, 3820 (1997).
[8] A.C. Ferrari, B. Kleinsorge, N.A. Morrison, A. Hart, V. Stolojan, and J. Robertson, J. Appl. Phys. **85**, 7191 (1999).
[9] R. Kalish, Y. Lifshitz, K. Nugent, and S. Prawer, Appl. Phys. Lett. **74**, 2936 (1999).
[10] J.P. Sullivan, T.A. Friedmann, and A.G. Baca, J. Electron. Mater. **26**, 1021 (1997).
[11] M. Gioti, S. Logothetidis, and C. Charitidis, Appl. Phys. Lett. **73**, 184 (1998).
[12] S. Logothetidis, M. Gioti, C. Charitidis, P. Patsalas, J. Arvanitidis, and J. Stoemenos, Appl. Surf. Sci. **138-139**, 244 (1999); S. Logothetidis, M. Gioti, C. Charitidis, and P. Patsalas, Vacuum **53**, 61 (1999).
[13] N. Metropolis, A.W. Rosenbluth, M.N. Rosenbluth, A.H. Teller, and E. Teller, J. Chem. Phys. **21**, 1087 (1953).
[14] J. Tersoff, Phys. Rev. B **39**, 5566 (1989).
[15] P.C. Kelires, Phys. Rev. Lett. **75**, 1114 (1995).
[16] P.C. Kelires and E. Kaxiras, Phys. Rev. Lett. **78**, 3479 (1997).
[17] M.J. Mehl, J.E. Osburn, D.A. Papaconstantopoulos, and B.M. Klein, Phys. Rev. B **41**, 10 311 (1990).
[18] S. Logothetidis, Appl. Phys. Lett. **69**, 158 (1996).
[19] S. Logothetidis, M. Gioti, P. Patsalas, and C. Charitidis, Carbon **37**, 765 (1999).
[20] See for example, M. Chhowalla, J. Roberston, C.W. Chen, S.R.P. Silva, C.A. Davis, G.A.J. Amaratunga, and W.I. Milne, J. Appl. Phys. **81**, 139 (1997).
[21] S. Logothetidis, C. Charitidis, and P. Patsalas, Diamond Relat. Mater. (to be published).
[22] Y. Lifshitz, S.R. Kasi, J.W. Rabalais, and W. Eckstein, Phys. Rev. B **41**, 10 468 (1990).
[23] C.A. Davis, Thin Solid Films **226**, 30 (1993).
[24] J. Schwan, S. Ulrich, H. Roth, H. Erhardt, P. Becker, and S.R.P. Silva, J. Appl. Phys. **82**, 6024 (1997).
[25] E. Mounier and Y. Pauleau, Diamond Relat. Mater. **6**, 1182 (1997).
[26] P. Patsalas, M. Handrea, S. Logothetidis, M. Gioti, S. Kennou, and W. Kautek, Diamond Relat. Mater. **10**, 960 (2001).
[27] P. Patsalas and S. Logothetidis, Nucl. Instrum. Methods Phys. Res. B **178**, 247 (2001).
[28] R. M. A. Azzam and N. Bashara, *Ellipsometry and Polarized Light* (North-Holland, Amsterdam, 1977).
[29] D.E. Aspnes, Thin Solid Films **89**, 249 (1982).
[30] S. Logothetidis, J. Petalas, and S. Ves, J. Appl. Phys. **79**, 1040 (1996).
[31] F. Xiong, Y.Y. Wang, and R.P.H. Chang, Phys. Rev. B **48**, 8016 (1993).
[32] A.C. Ferrari, A. Libassi, B.K. Tanner, V. Stolojan, J. Yuan, L.M. Brown, S.E. Rodil, B. Kleinsorge, and J. Robertson, Phys. Rev. B **62**, 11 089 (2000).
[33] C.A. Lucas, T.D. Nguyen, and J.B. Kortright, Appl. Phys. Lett. **59**, 2100 (1991).
[34] Y. Huai, R.W. Cochrane, and M. Sutton, Phys. Rev. B **48**, 2568 (1993).
[35] D.E. Savage, J. Kleiner, N. Schimke, Y.H. Phang, T. Jankowski, J. Jacobs, R. Darious, and M.G. Lagally, J. Appl. Phys. **69**, 1411 (1991).
[36] J.B. Kortright, J. Appl. Phys. **70**, 3620 (1991).
[37] H. Schuster and H. Goebel, Adv. X-Ray Anal. **39**, 1 (1996).
[38] P. Patsalas and S. Logothetidis, J. Appl. Phys. **88**, 6346 (2000).
[39] R.J. Jaccodine and W.A. Schlegel, J. Appl. Phys. **37**, 2429 (1966).
[40] W.C. Oliver and G.M. Pharr, J. Mater. Res. **7**, 1564 (1992).
[41] S. Logothetidis and C. Charitidis, Thin Solid Films **353**, 208 (1999).
[42] P.C. Kelires, Phys. Rev. Lett. **68**, 1854 (1992).
[43] N.A. Marks, Phys. Rev. B **63**, 035401 (2000).
[44] U. Stephan and M. Haase, J. Phys.: Condens. Matter **5**, 9157 (1993).
[45] H.-P. Kaukonen and R.M. Nieminen, Phys. Rev. Lett. **68**, 620 (1992).
[46] H.U. Jager and K. Albe, J. Appl. Phys. **88**, 1129 (2000).
[47] N.A. Marks, D.R. McKenzie, B.A. Pailthorpe, M. Bernasconi, and M. Parrinello, Phys. Rev. Lett. **76**, 768 (1996).
[48] D.G. McCulloch, D.R. McKenzie, and C.M. Goringe, Phys. Rev. B **61**, 2349 (2000).
[49] C.A. Davis, G.A.J. Amaratunga, and K.M. Knowles, Phys. Rev. Lett. **80**, 3280 (1998).
[50] P.C. Kelires, J. Non-Cryst. Solids **227-230**, 597 (1998).
[51] R. Haerle, A. Baldereschi, and G. Galli, J. Non-Cryst. Solids **266-269**, 740 (2000).
[52] There is some uncertainty in the computed stresses, as is pointed out earlier (Ref. 6), because of the use in their defining equation of a unique atomic volume Ω_i for both sp^3 and sp^2 sites. In general, sp^2 (sp^3) sites have a larger (smaller) Ω_i than the mean value used here (obtained by dividing the volume of the cell with the total number of atoms), and this leads to overestimation (underestimation) of the magnitude of stresses of sp^2 (sp^3) sites, respectively, by about 20% for the sp^2 sites and 10% for the sp^3 sites.
[53] A.K. Bhattacharya and W.D. Nix, Int. J. Solids Struct. **24**, 1287 (1998).
[54] P.C. Kelires, Diamond Relat. Mater. **10**, 139 (2001).
[55] A.C. Ferrari, J. Robertson, M.G. Beghi, C.E. Bottani, R. Ferulano, and R. Pastorelli, Appl. Phys. Lett. **75**, 1893 (1999).
[56] M.H. Manghnani, S. Tkachev, P.V. Zinin, X. Zhang, V.V. Brazhkin, A.G. Lyapin, and I.A. Trojan, Phys. Rev. B **64**, 121403 (2001).
[57] R. Pastorelli, P.M. Ossi, C.E. Bottani, R. Checchetto, and A. Miotello, Appl. Phys. Lett. **77**, 2168 (2000).
[58] E. Martinez, J.L. Andujar, M.C. Polo, J. Esteve, J. Robertson, and W.I. Milne, Diamond Relat. Mater. **10**, 145 (2001).

[59] P. Patsalas, S. Logothetidis, P. Douka, M. Gioti, G. Stergioudis, Ph. Komninou, G. Nouèt, and Th. Karakostas, Carbon **37**, 865 (1999).
[60] M.P. Siegal, D.R. Tallant, P.P. Provencio, D.L. Overmyer, R.L. Simpson, and L.J. Martinez-Miranda, Appl. Phys. Lett. **76**, 3052 (2000).
[61] L.J. Martinez-Miranda, M.P. Siegal, and P.P. Provencio, Appl. Phys. Lett. **79**, 542 (2001).